מכון ויצמן למדע

WEIZMANN INSTITUTE OF SCIENCE

Thesis for the degree
Master of Science

חבור לשם קבלת התואר
מוסמך למדעים

By
Amit Finkler

מאת
עמית פינקלר

התקן התאבכות על-מוליכים על חוד: כלי לחקר חומר מערבולתי בעל-מוליכים של טמפרטורות גבוהות
A SQUID on a tip:
A tool to explore vortex matter in high-Tc superconductors

Advisors
Prof. Amir Yacoby and Prof. Eli Zeldov

מנחים
פרופ' עמיר יעקבי ופרופ' אלי זלדוב

November 2006

חשון ה'תשס"ז

Submitted to the Scientific Council of the
Weizmann Institute of Science
Rehovot, Israel

מוגש למועצה המדעית של
מכון ויצמן למדע
רחובות, ישראל

Abstract

Scanning probe microscopes (SPM) have been used to explore many interesting physical properties of matter. Of these, the Scanning tunneling microscope (STM) and the atomic force microscope (AFM) are well-known, and today there is a large variety of SPMs, each being able to measure locally a unique property of matter, such as compressibility, magnetic force, spectra, etc.

An SPM based on a superconducting quantum interference device (SQUID) was first built by Rogers and Bermon in the early 1980s. This kind of microscope combines the superb magnetic field sensitivity a SQUID can offer with finely-tuned spatial resolution a scanning system possesses. The SQUIDs used in these microscopes are normally fabricated in a clean-room process on a planar substrate.

In this work we explored the possibility of fabricating a SQUID on the edge of a submicron conical tip. The advantage of using a tip instead of a planar substrate as a probe is that one can approach the surface of a sample more accurately and the ease of making SQUIDs which are typically much smaller than standard planar ones. As a first step we made $Al/Al_2O_3/Al$ Josephson junctions on tips with a diameter of 100nm and 500nm and afterwards succeeded in producing high-quality reproducible aluminium SQUIDs on tips having a diameter of 300nm. These SQUIDs had a sensitivity of less than $10^{-3}\Phi_0/\sqrt{\text{Hz}}$ at a temperature of 300mK. We have also begun to work on making SQUIDs out of niobium, which we will be able to operate at temperatures above 4.2K.

We intend to use this 'SQUID on a tip' as a sensor to locally probe the magnetic flux of single vortices in high-T_C superconductors and possibly single molecule magnets by inserting it into a scanning probe microscope.

Contents

List of Figures

1. Introduction

Since the discovery of high-T_C superconductors in 1986 by Müller and Bendorz [1], there has been great interest in the field. Specifically, vortex matter has been the research subject of many groups and continues to give us intriguing and stimulating results. In this chapter we will give a brief introduction about the two main types of superconductivity and present the motivation for this work and its goal.

1.1 Type I Superconductors

Aside from the phase transition from a normal metal to a superconducting one at a critical temperature T_c, type I superconductors exhibit two additional critical quantities[1], the critical current density J_c and the critical field H_c, above which the superconductor reverts back to a normal metal. Using the Ginzburg-Landau equations, the critical field is given by

$$H_c(T) = \frac{\Phi_0}{\sqrt{8}\pi\xi(T)\lambda(T)}, \tag{1.1}$$

where Φ_0 is the flux quantum, $\Phi_0 = h/2e$, ξ is the coherence length and λ is the effective magnetic field penetration length.

1.2 Magnetic Properties of Type II Superconductors

In these materials, an intermediate phase exists between the truly superconducting state and the normal state, also known as the vortex state. In this state, magnetic flux penetrates the superconductor in the form of a periodic vortex lattice, first predicted by Abrikosov [2]. Each such vortex carries a single flux quantum, Φ_0. This state exists in a specific magnetic field

1 Both depend on the temperature.

range, $H_{c1} < H < H_{c2}$, where

$$H_{c1} = \frac{\Phi_0}{4\pi\lambda^2} \log \kappa \quad ; \quad \kappa = \lambda/\xi \tag{1.2}$$

$$H_{c2} = \frac{\Phi_0}{2\pi\xi^2}. \tag{1.3}$$

Measuring such a material with a magnetic flux sensor enables us to image the vortex lattice [3, 4]. This has been suggested and experimentally shown by numerous groups throughout the years. The methods are many, and the variety of magnetic field and spatial sensitivity is rather large. Of these methods, we mention Bitter decoration, magneto-optics, the Hall effect and quantum interference devices (Josephson junctions, SQUIDs).[5, 6, 7]
A graphical comparison of these techniques was given by Bending [8], which we reproduce in fig. 1.1. In the last few years there have been reports of planar SQUIDs with an area as small as 1μm x 1μm [9] and smaller.

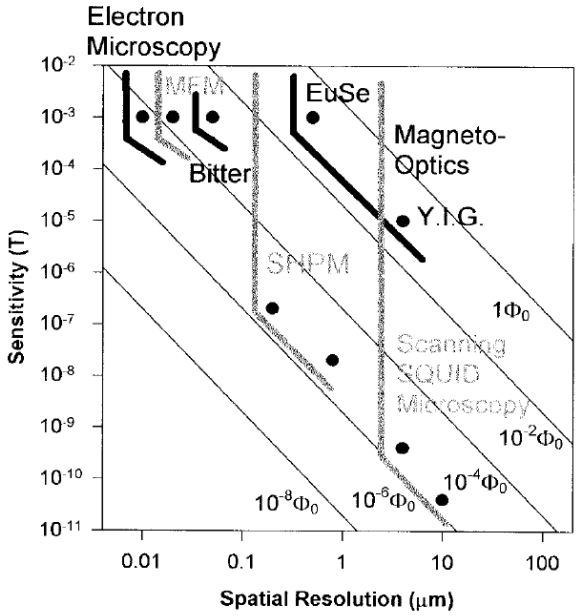

Fig. 1.1: *A graphical comparison by Bending [8] from 1999 of different magnetic field sensors by sensitivity and spatial resolution. SHPM is scanning Hall probe microscopy; YIG and EuSe are specific magneto-optical materials.*

1.3 Goal

We wish to produce a local magnetic field sensor for a scanning probe microscope (SPM). The purpose of this sensor is to investigate the physics of vortex matter. The required specifications of this sensor should be:

1. Small size (spatial resolution). The distance between vortices in an applied magnetic field of 20 Gauss is 1μm. A reasonable requirement is then to have a size of several hundred nanometers.

2. High sensitivity (magnetic field modulation). At a distance of a few tens of nanometers above the surface of a superconducting crystal, the modulation between the magnetic field in an isolated vortex and outside of it is ∼100 Gauss and much lower at higher fields. Therefore, we want the sensor to have a < 1 Gauss$/\sqrt{\text{Hz}}$ sensitivity.

3. Ease of approach of the sensor to the sample.

4. Operation temperature of 300mK for an aluminium sensor and 1.5K-4K for a niobium sensor. These are actually requirements that stem from the metals we are working with, but nonetheless they impose limitations on our system.

To implement these specifications we attempted to make a SQUID on a tip. Our starting point was a proved capability of producing an SET on a tip, so that what we needed were some modifications of the existing single electron transistor on a tip (SET) process [10]:

1. Tip-making procedure for various tip diameters

2. Evaporation and oxidation stages - Josephson junctions and SQUIDs

3. A new tip holder which would serve both for evaproation and for measurement

4. A measurement rod for a helium-3 system

1.4 Units

In this work we shall use the SI system of units, unless otherwise mentioned.

2. Theory

2.1 Superconductor-Insulator-Superconductor Tunneling

To give a fairly intuitive understanding of quasi-particle tunneling in a superconductor-insulating-superconductor junction (SIS), we will employ the semiconductor model [11]. Superconductors are represented as semiconductors, where the gap energy is 2Δ. A typical tunnel junction between two superconductors is illustrated in fig. 2.1.

Using the independent-particle approximation, the quasiparticle tunneling current between the two superconductors is

$$I_{1\to 2} = A \int_{-\infty}^{\infty} |T|^2 g_1(E) f(E) g_2(E+eV)[1-f(E+eV)]\mathrm{d}E. \tag{2.1}$$

Here A is a constant, V is the voltage bias and T is the tunneling matrix element (assumed to be a constant), g_1, g_2 are the densities of states and $f(E)$ is the Fermi-Dirac distribution function. For superconductors we need to replace g_1 and g_2 with the superconductors' density of states, so that the tunneling current becomes

$$I_{ss} = \frac{G_n}{e} \int_{-\infty}^{\infty} \Re\left\{ \frac{|E|}{\sqrt{E^2-\Delta_1^2}} \right\} \times \\ \times \ \Re\left\{ \frac{|E+eV|}{\sqrt{(E+eV)^2-\Delta_2^2}} \right\} [f(E)-f(E+eV)]\,\mathrm{d}E. \tag{2.2}$$

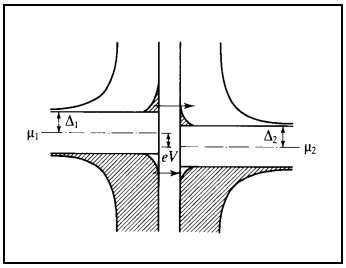

Fig. 2.1: *Typical SIS tunnel junction in the semiconductor model for $T > 0$. Note that superconductor 1 is biased with respect to superconductor 2. The figure was taken from [11].*

In the above equation we replaced the constants with a rather important physical quantity, the normal state conductance G_n. In all of our discussion below, we will take $\Delta_1 = \Delta_2 \equiv \Delta$ as this was the only case treated in this work. The corresponding V-I curve for an SIS tunnel junction is illustrated in fig. 2.2. No quasiparticle current can flow between the two superconductors at $T = 0$ for $V < 2\Delta/e$. This is clear from fig. 2.1, since we need to overcome the gap of

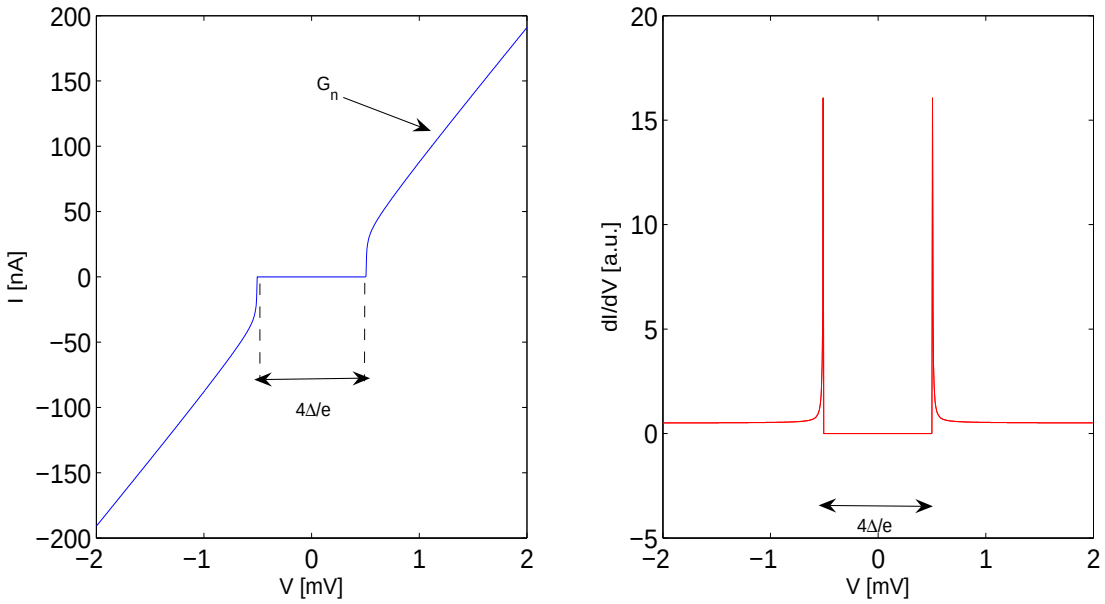

Fig. 2.2: *Calculation of I-V characteristics for superconductor-insulator-superconductor tunneling for aluminium with* $\Delta = 250\mu\text{eV}$ *and* $R_n = 10\text{k}\Omega$ *at 300mK.*

both superconductors. At finite temperatures, however, quasiparticles with energy above the gap energy will give rise to a subgap current. Two important quantities can be found from this graph: the normal state conductance, G_n (or resistance R_n), and the superconducting gap, Δ. The differential conductance measures the density of states of the two superconductors in low temperatures and the zero-current gap equals exactly 4Δ (in a symmetric graph with both positive and negative voltages. Otherwise it is 2Δ.)

2.2 The Josephson Effect

2.2.1 T = 0

Basics

Predicted by Brian D. Josephson [12] in 1962, a "supercurrent" should flow between two superconductors separated by a thin insulating barrier at zero voltage bias. This barrier can be generalized to some weak link [13], be it a normal metal proximity layer, an insulating oxide barrier or some geometrical constriction between the two superconductors. The observation of this supercurrent is a mark of the dc Josephson effect. It is given by

$$I_s = I_c \sin\gamma, \tag{2.3}$$

where I_c is the maximal supercurrent the junction can carry, hence termed the *critical current*, and γ is the *gauge-invariant* phase difference between the wave functions of the two superconductors,

$$\gamma = \Delta\varphi - \frac{2\pi}{\Phi_0}\int \mathbf{A}\cdot \mathrm{d}\mathbf{s}, \tag{2.4}$$

for the gauge-variant phase difference $\Delta\varphi$. The supercurrent can be measured directly, illustrated by a measurement by Steinbach et al. [14] in fig. 2.3.

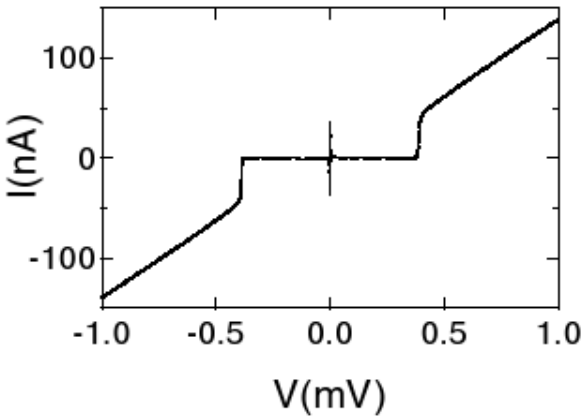

Fig. 2.3: *Direct measurement of a Josephson supercurrent by Steinbach et al. [14].*

Another prediction of Josephson is, that at finite voltage bias, the phase will evolve in time according to

$$\frac{d\gamma}{dt} = \frac{2eV}{\hbar}, \tag{2.5}$$

commonly known as the ac Josephson effect.

RCSJ model

One can model a real Josephson junction by an ideal junction which is connected to a resistor R and a capacitor C, both in parallel. The resistance represents dissipation at finite voltage bias and the capacitance is the geometrical capacitance between the two superconductors.[1] Therefore, in the RCSJ model the current can be written as

$$I = I_{c0}\sin\gamma + \tfrac{V}{R} + C\tfrac{dV}{dt}. \tag{2.6}$$

1 Josephson predicted yet another dissipative term which is a result of Cooper pair-quasi particle interference, but since it is rather difficult to measure, we shall omit its effect in our discussion.

Substituting eq. 2.5 in eq. 2.6 and introducing a dimensionless time variable $\tau = \sqrt{\frac{2eI_{c0}}{\hbar C}}t$, one derives the following differential equation for γ:

$$\frac{d^2\gamma}{d\tau^2} + \frac{1}{Q}\frac{d\gamma}{d\tau} + \sin\gamma = \frac{I}{I_{c0}}. \tag{2.7}$$

An important quantity, Q, the quality factor, was introduced above, $Q = \sqrt{\frac{2eI_{c0}}{\hbar C}}RC$, as the characteristics of the tunnel junction change substantially from the overdamped ($Q \ll 1$) to the underdamped ($Q > 1$) regime. In the overdamped regime, eq. 2.6 reduces to

$$\frac{d\gamma}{dt} = \frac{2eI_{c0}R}{\hbar}\left(\frac{I}{I_{c0}} - \sin\gamma\right). \tag{2.8}$$

Integrating this equation and using eq. 2.5 for a phase advancement of 2π gives us the relation

$$V = R\sqrt{I^2 - I_{c0}^2}. \tag{2.9}$$

I_{c0} is the observed critical current, which may be smaller than the maximal critical current [14]. In the underdamped regime, the I-V curve will exhibit hysteresis. Overdamped and underdamped I-V curves are displayed in fig. 2.4. The right figure is taken from Tinkham [11].

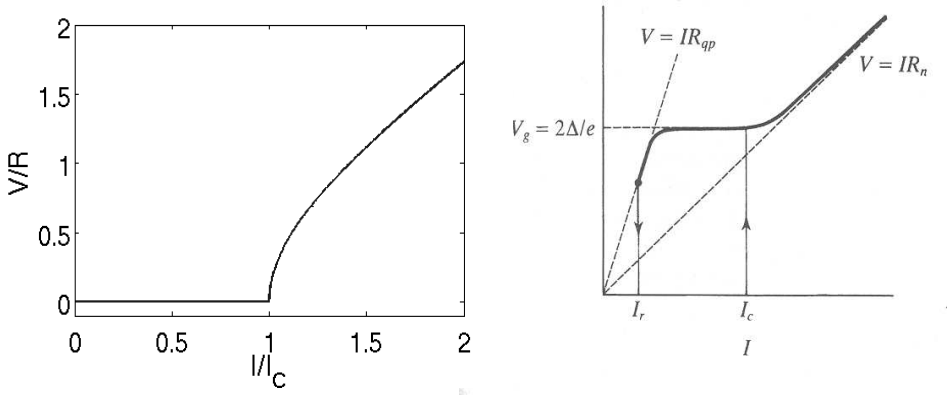

Fig. 2.4: *I-V characteristics of a Josephson junction according to the RCSJ model. Left figure: an overdamped junction. Right figure: an underdamped junction.*

2.2.2 Thermal fluctuations

The first examination of the thermal noise in the dc Josephson effect was reported by Ambegaokar and Halperin [15], who added to the above RCSJ model an additional fluctuating noise current, so that the equation for the current becomes

$$I = I_{c0}(T)\sin\gamma + \tfrac{V}{R} + C\tfrac{dV}{dt} - \bar{L}(t), \tag{2.10}$$

and the thermal noise obeys $\langle \bar{L}(t+\tau)\bar{L}(t)\rangle = \frac{2R}{T}\delta(\tau)$. For a shunted junction (as in the RCSJ model), they got current-voltage characteristics which were illustrated very clearly by Falco et al.[16] in fig. 2.5. It is important to note that these fluctuations are important when the

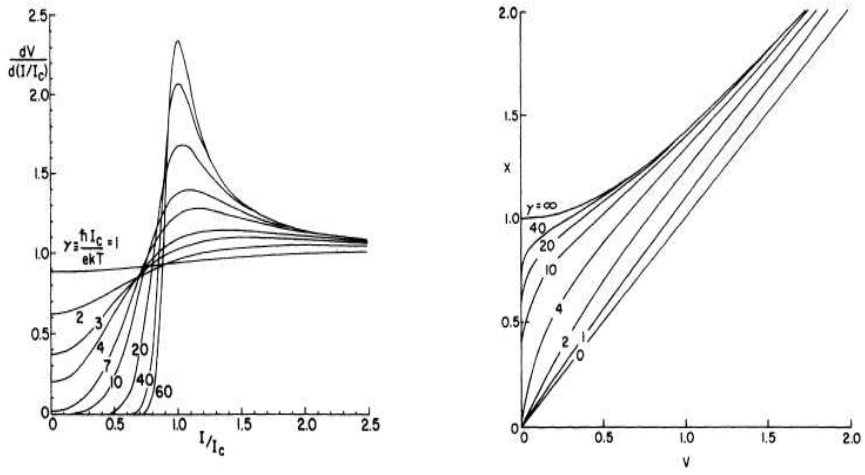

Fig. 2.5: *On the left, the differential resistance dV/dI as a function of the same current from the right-hand figure. On the right, V-I characteristics for a shunted Josephson junction with thermal noise taken into account.*

Josephson energy, $E_J = \frac{G_n R_Q}{2}\Delta$ [17], [2], is of the same order of magnitude (or smaller) as the thermal energy $k_B T$. Eq. 2.9 then changes significantly, i.e. there will always be a finite resistance for $T > 0$ even if $I < I_c$. This finite resistance approaches $R_0 = R_n \frac{\hbar I_{c0}}{e k_B T} e^{-\frac{\hbar I_{c0}}{e k_B T}}$ as $I \to 0$.

2.2.3 Magnetic field dependence

To see the physical beauty of Josephson junctions, one must place them in a magnetic field. For simplicity we will consider a junction having a rectangular cross-section in the $x-z$ plane with an applied field in the z-direction, but this applies to any geometrical form. The supercurrent flows in the y direction through the junction and can be written as

$$I_s = \iint J_c(x,z)\sin\gamma(x)\mathrm{d}x\mathrm{d}z, \tag{2.11}$$

the integration being on the cross-section of the junction. Since γ is independent of z, we may integrate it to get

$$I_s = \int \mathcal{J}_c(x)\sin\gamma(x)\mathrm{d}x. \tag{2.12}$$

2 $R_Q = h/(2e)^2 \simeq 6.5k\Omega$ is the resistance quantum for a Cooper pair

From eq. 2.4 we know that the phase difference between the two superconductors is periodic in the magnetic flux, Φ, so that in the end [3] the magnetic field dependence of the maximal critical current is

$$I_m(\Phi) = I_m(0)\left|\frac{\sin(\pi\Phi/\Phi_0)}{\pi\Phi/\Phi_0}\right|, \tag{2.13}$$

which is in effect the Fourier transform of the shape of the junction (see fig. 2.6).

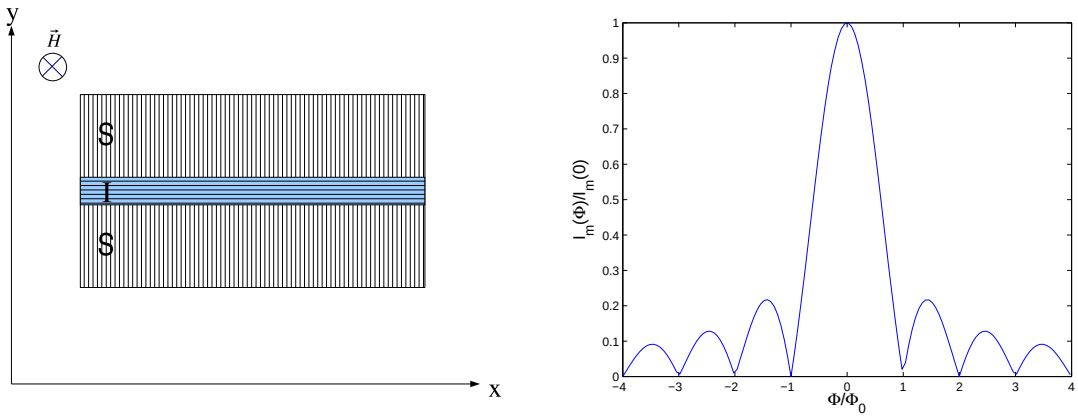

Fig. 2.6: *Magnetic field dependence of a rectangular (top-view given in the left figure) Josephson junction in reduced units (right figure).*

2.2.4 Small size effects

In sec. 2.2.1 we assumed that the circuit is biased by an ideal current source. However, one must consider the impedance of this alleged ideal current source at the typical frequency involved in the process, which is the plasma frequency $\omega_p = \sqrt{\frac{2eI_{c0}}{\hbar C}} \sim 10^{11}[\frac{\text{rad}}{\text{sec}}]$. At this high frequency, any regular leads to the real physical junction will have the typical transmission line impedance, i.e. $Z_1 \sim 377\Omega$ in free space. Therefore, we will observe damping in high frequencies for any measurement system which has normal transmission lines [18, 19, 20].[4] This situation is often called "phase diffusion", in which one would observe a finite resistance at currents below the critical current of the junction[5]. It was found [19] that this finite resistance is

$$\begin{cases} R_0 = \pi Z_1(2E_J/k_BT)e^{-2E_J/k_BT} & E_J \gg k_BT \\ R_0 = 2Z_1(k_BT/E_J)^2 & E_J \ll k_BT \\ R_0 = \frac{Z_1}{I_0^2(E_J/k_BT)-1} & \text{for a general } E_J. \end{cases} \tag{2.14}$$

3 see [11] for a detailed derivation

4 Interestingly, a recent work succeeded in doing the opposite, see [14].

5 This is actually an alternative theory for thermal fluctuations shown in sec. 2.2.2.

Here $I_0(x)$ is the zeroth order modified Bessel function. A similar treatment is given by Ivanchenko and Zil'berman [21, 22],

$$I(V_B) = I_c \Im \left[\frac{I_{1-i2\beta eV_B/\hbar R_B}(\beta E_J)}{I_{-i2\beta eV_B/\hbar R_B}(\beta E_J)} \right], \tag{2.15}$$

where I_ν is the modified Bessel function, $\beta = (k_B T)^{-1}$ and $V_B = V + R_B I$. R_B is the total resistance seen by the junction [14][6]. Both works reach the conclusion that for $E_J \ll k_B T$, the current is given by

$$I(V) = \frac{1}{2} I_{c0}^2 \frac{Z_1 V}{V^2 + (2eZ_1 k_B T/\hbar)^2}, \tag{2.16}$$

which is illustrated in fig. 2.7 from [17]. Therefore, in the phase diffusion regime we expect

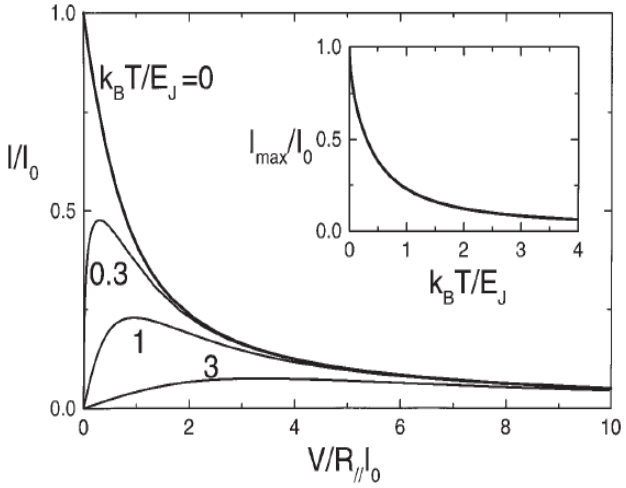

Fig. 2.7: *I-V characteristics of a junction coupled to the environment, taken from [17]. At high voltage biases, all curves coincide since then* $I(V) \sim \frac{1}{2} I_{c0}^2 Z_1 \frac{1}{V}$ *(see eq. 2.16).*

to observe a smearing of the supercurrent such that it will occur at a small finite voltage bias. Since resistance goes inversely with the junction area and since the Josephson energy E_J is inversely proportional to R_n, we now understand that once one takes the environment of the junction into consideration, the Josephson effect can show a profound dependence on the junction's size. This is especially important in small junctions, where E_J becomes significantly small with respect to the thermal energy.

2.3 Superconducting QUantum Interference Device : SQUID

First measured by Jalkevic, Lambe, Silver and Mercereau [23, 24], hence in the first days it was known as the "Mercereau Effect". A SQUID is just two Josephson junctions connected in

6 there's also an external capacitance, C_B, seen by the junction

parallel. In the following analysis we ignore the effect of magnetic field on the superconducting electrodes and commit ourselves only to its effect on the junctions. Let us consider the geometrical setup illustrated in fig. 2.8. We consider then the line integral of the vector potential **A**

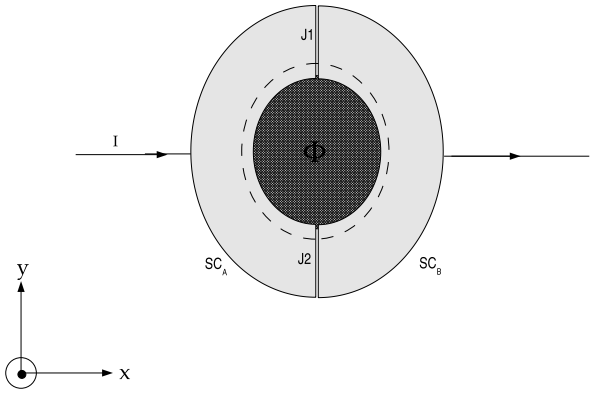

Fig. 2.8: *SQUID scheme. The maximal supercurrent through this device obeys* $I_{max} = 2I_c|\cos(\pi\Phi/\Phi_0)|$.

around the contour denoted by the dashed line, going through both superconductors, SC_A, SC_B and both junctions, J_1, J_2. This integral must equal the flux Φ passing through the contour. If we take $\mathbf{A} = \frac{\Phi_0}{2\pi}\nabla\varphi$ in the superconductors then the total flux will be

$$\Phi = \oint \mathbf{A}\cdot \mathrm{d}\mathbf{s} = \frac{\Phi_0}{2\pi}\int\limits_{\text{electrodes}} \nabla\varphi\cdot \mathrm{d}\mathbf{s} + \int\limits_{\text{junctions}} \mathbf{A}\cdot \mathrm{d}\mathbf{s}. \tag{2.17}$$

As φ must be single-valued, a complete contour of φ including the phase differences across the junctions, $\Delta\varphi_i$ should be zero modulo 2π. This means we can replace $\frac{\Phi_0}{2\pi}\int\limits_{\text{electrodes}} \nabla\varphi\cdot \mathrm{d}s$ with $-\sum_i \Delta\phi_i \mod 2\pi$. Consequently, eq. 2.17 becomes

$$\Phi = -\frac{\Phi_0}{2\pi}\sum_i \Delta\phi_i \mod 2\pi + \int\limits_{\text{junctions}} \mathbf{A}\cdot \mathrm{d}s. \tag{2.18}$$

Using eq. 2.4 in eq. 2.18, we finally find that

$$\gamma_1 - \gamma_2 = \frac{2\pi\Phi}{\Phi_0} \mod 2\pi. \tag{2.19}$$

Here both γ_1 and γ_2 are defined as the phase difference from SC_A to SC_B. This last equation shows us that for $\gamma_1 = \gamma_2$, Φ must be an integral multiple of Φ_0. If $\gamma_1 = \gamma_2 = \pi/2$, the

supercurrent will attain its maximal value (see eq. 2.3). Let us now calculate the maximal critical current using eqs. 2.3 and 2.19 assuming $I_{c2} < I_{c1}$:

$$I_m = I_1 + I_2 = I_{c1}\sin\gamma_1 + I_{c2}\sin\gamma_2 = I_c\sin\gamma_1 + 2I_{c2}\sin\left(\frac{\gamma_1+\gamma_2}{2}\right)\cos\left(\frac{\gamma_1-\gamma_2}{2}\right) = \quad (2.20)$$

$$= I_c\sin\gamma_1 + 2I_{c2}\sin\left(\frac{\pi}{2}\right)\cos\left(\frac{\pi\Phi}{\Phi_0}\right) = I_c\sin\gamma_1 + 2I_c\cos\left(\frac{\pi\Phi}{\Phi_0}\right). \quad (2.21)$$

Here $I_{c1} \equiv I_{c2} + I_c$. Obviously, for $I_{c1} = I_{c2}$ eq. 2.21 reduces to

$$I_{\max} = 2I_c\left|\cos\left(\frac{\pi\Phi}{\Phi_0}\right)\right|. \quad (2.22)$$

This result can be used to calculate the magnetic flux through a loop by measuring the critical current, which results in resolving the magnetic flux to very accurate values (as accurate as $10^{-6}\Phi_0$). In the ideal case, then, the critical current modulates between $2I_c$ and 0. However, as the SQUID's inductance increases, this modulation depth decreases, since it becomes more and more difficult for the current to compensate for the total flux. It can be shown (ref. [25]) that the minimum critical current is of the order of $2(I_c - \Phi_0/2L)$, with L being the SQUID inductance.

Just as in section 2.2.3, one could have found the magnetic field dependence by calculating the Fourier transform in the $y-z$ plane of the device's geometry. Note, that in the present case the device is analogous to a two-slit mask, where each slit corresponds to a Josephson junction of length l and width w and they are separated a distance d apart. The Fourier transform of such a two-slit mask is

$$\mathcal{F}(k) = 4\cos(kd/2)\frac{\sin(kl/2)}{k}. \quad (2.23)$$

In this expression we identify the $\cos(kd/2)$ term with the oscillating part from eq. 2.21 and we see that there's also a decaying oscillatory envelope, whose period will be observable if the size of the junctions (slits) is of the same order of magnitude as the SQUID's diameter (distance between the slits).

3. Experimental Setup

3.1 Tip Processing

We use quartz (fused SiO_2) rods and tubes with an outer diameter of 1mm. For the tubes, their inner diameter is 0.5mm. The rods/tubes were purchased from Sutter Instrument (Heraeus HSQ300). Compared to other glasses, quartz has the lowest dielectrical constant, the highest volume resistivity, a high melting point and a small thermal expansion coefficient.

3.1.1 Tip pulling

In order to pull quartz we use Sutter Instrument's CO_2 laser-based micropipette puller, model P-2000. To pull rods we used two distinct recipes [26, 27], which give one tip with a diameter of 70nm at its end and another with a diameter of 500nm at its end.
The pulled tubes used had an outer diameter of $\sim$300nm and an inner diameter of $<$100nm.

3.1.2 Evaporation

Aluminium

All aluminium tips were evaporated in an Edwards thermal evaporator at a background pressure of $1.5 \cdot 10^{-6}$ Torr. The tips were placed in a designated rotator flange, which enables the rotation of the tip with respect to the evaporation source. Zero-angle alignment was done using a small laser diode placed next to the rotating frame. Each superconducting device was fabricated in a different process, where the main differences are the angle of evaporation and whether or not in-situ oxidation was used in the process. In addition, we were able to measure the tip's resistance during the process using in-vacuum wiring going from the tip-holder to the electrical feedthrough. The evaporation consisted of several steps:

- Continuous film rod tips

    1. 200Å at an angle of 100° with respect to the source.

2. 200Å at an angle of -100° with respect to the source.
3. 200Å at an angle of 0° with respect to the source.

These tips are the simplest to make and involve no oxidation.

- Josephson tunnel junction rod tips, geometry #1
  1. 200Å at an angle of 100° with respect to the source.
  2. Oxidation with synthetic air for 30 seconds at a pressure of 100mTorr.
  3. 200Å at an angle of -100° with respect to the source.
  4. 200Å at an angle of 0° with respect to the source.

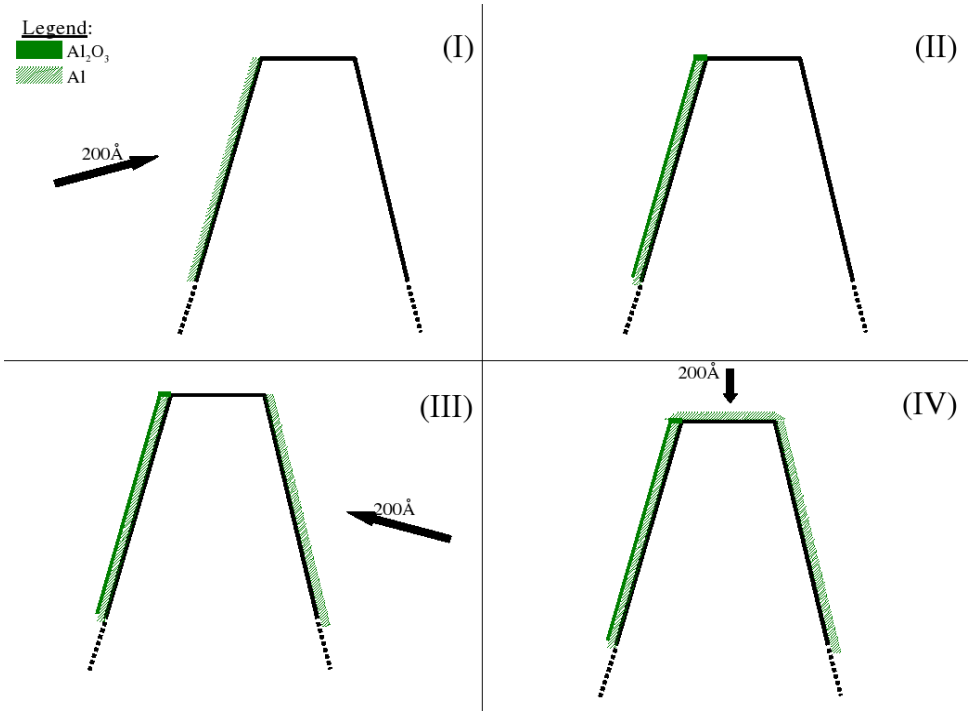

Fig. 3.1: *Josephson tunnel junction - evaporation geometry no. 1.*

- Josephson tunnel junction rod tips, geometry #2
  1. 225Å at an angle of 55° with respect to the source.
  2. Oxidation with synthetic air for 30 seconds at a pressure of 100mTorr.
  3. 225Å at an angle of -55° with respect to the source.

The differences between the two geometries are the alignment of the junction with respect to a magnetic field in the z-direction (perpendicular to the tip's end) and the effective

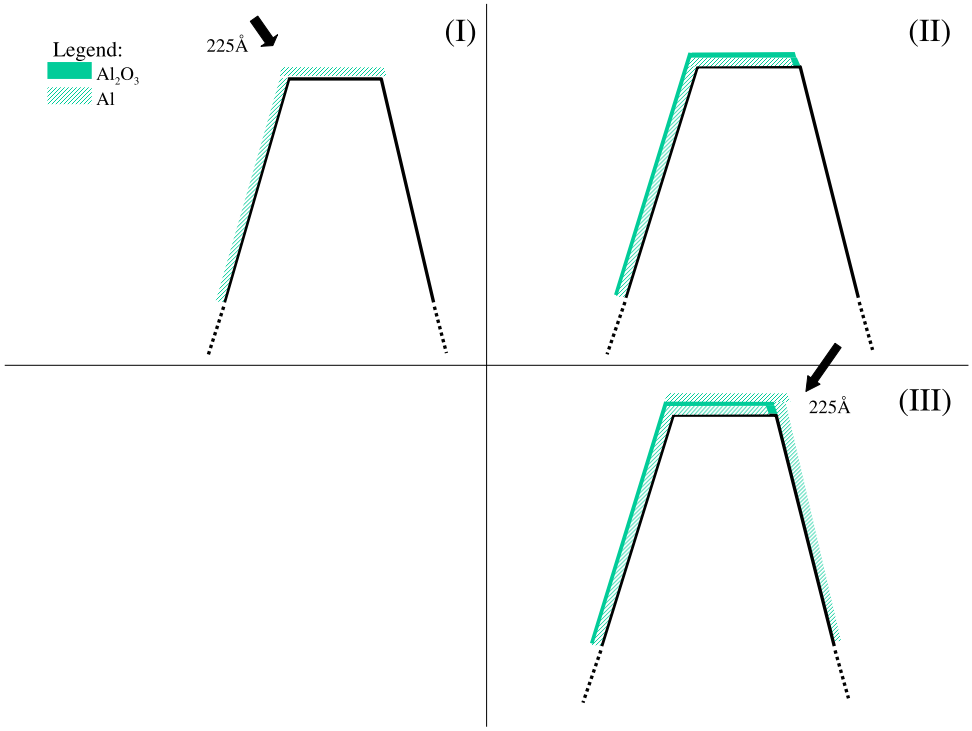

Fig. 3.2: *Josephson tunnel junction - evaporation geometry no. 2.*

size of the junction. Geometry no.1 was supposed to give a junction which is parallel to the magnetic field and geometry no.2 - perpendicular.

- SQUID tube tips

  1. 200Å at an angle of 100° with respect to the source.
  2. 200Å at an angle of -100° with respect to the source.
  3. 200Å at an angle of 0° with respect to the source.

An example of an evaporated tip is given in the SEM micrographs given in fig. 3.5. To illustrate the SQUID geometry in a different way, we plotted the SQUID viewed from the top in a stretched view, given in fig. 3.4.

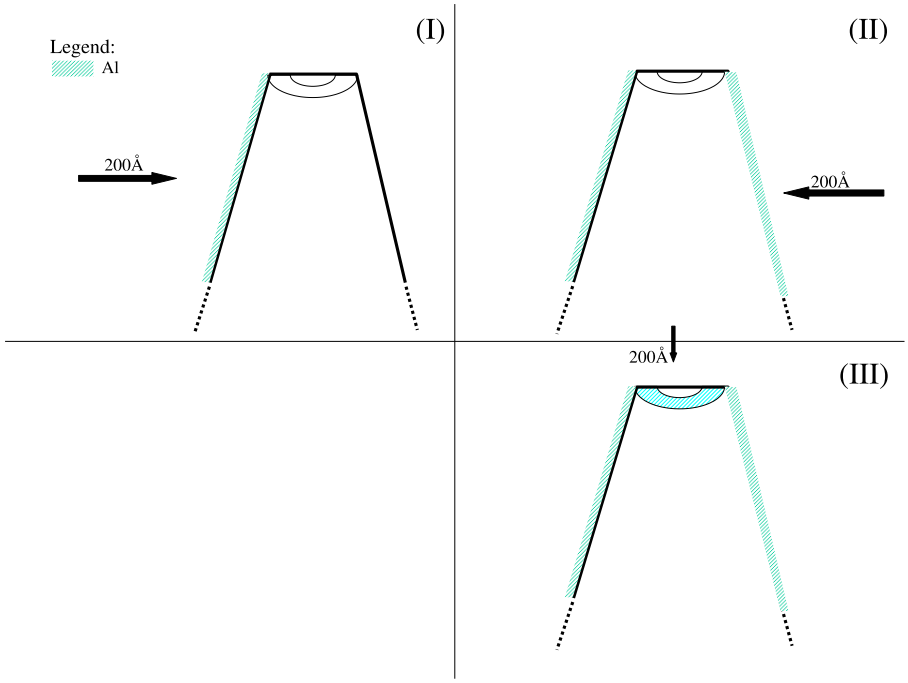

Fig. 3.3: *SQUID evaporation geometry*

Niobium

To evaporate niobium, we could not use the thermal evaporator since its crucible cannot reach the melting temperature of niobium, which is ∼3000°K for pure Nb. Therefore, we used an e-gun evaporator[1]. Apparently, to get thin superconducting niobium films in an e-gun evaporator, one should keep the substrate at a rather high temperature, i.e. from 400°C to 800°C during the evaporation [28, 29, 30, 31]. We managed to get a superconducting niobium thin film on a planar substrate as well as on a quartz tip. As there was no rotating device for this evaporator, we made one with substrate heating capabilities.

1 Vacuum Science Technology, `http://www.vstser.com`

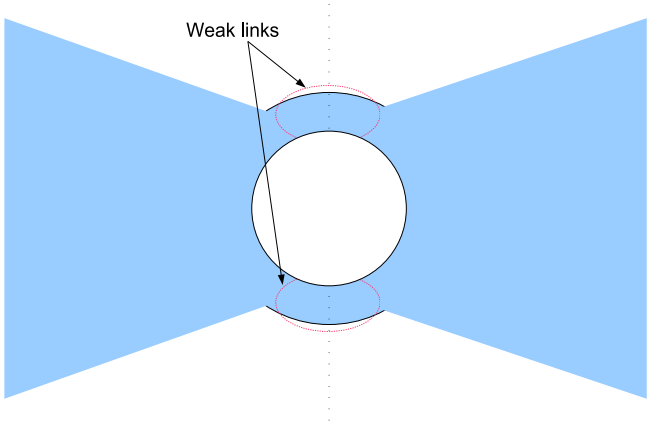

Fig. 3.4: *Stretched top view of a SQUID on a tip. The two large leads are from the left and from the right of the top of the tip. The areas encircled by a dashed red line are the weak links. For a 300nm tip diameter, the wall thickness is about 50nm, which naturally serves as a weak link.*

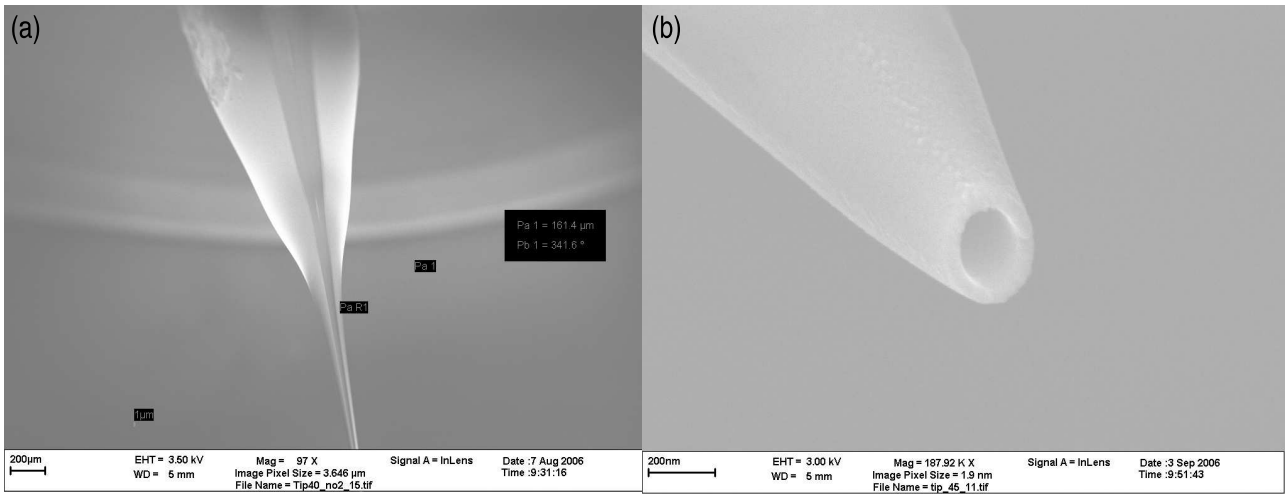

Fig. 3.5: *(a) A quartz tip evaporated with aluminium with a SQUID process. Note the dirty indium lead on the top left and the two aluminium leads on both sides of the tip; (b) A magnified image of the end of the tip from (a).*

3.2 Tip Holder

As our samples were not the usual planar substrates, we needed to make a unique tip holder, which will function both as a substrate (quartz tip) holder during evaporation and as a sample holder during low-temperature measurements in the liquid-helium systems. The design of our tip holder was based on an existing tip holder for the SPM. The idea is to use no direct wire-soldering to the tip and instead contact each side of the tip with a different electrode made out of brass or copper.

One electrode has a 1mm deep V-shaped groove where the tip fits, so that one side of the tip touches it, while a BeCu spring from the second electrode touches the other side of the tip. Since in each pulling process we get two tips, we designed a double-tip holder, illustrated in fig. 3.6. Copper wires are connected, either by soldering (for the aluminium tip holder) or by crimping (for the niobium tip holder), from the bottom pins to the electrodes. This way we could measure the tip's resistance during evaporation and afterwards use the same holder for low-temperature measurements.

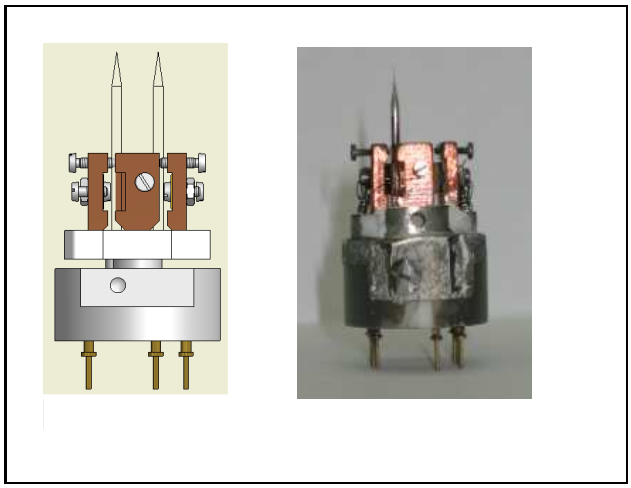

Fig. 3.6: *Our tip holder. Wires and adhesives are not displayed in the design on the left, but can be seen in the actual piece on the right.*

3.3 Helium-3, 300mK systems

Due to system availability considerations, the tips were measured in two different ^{3}He fridges. All of the continuous tips and few of the tunnel junction tips were measured in a "home-made", custom fridge[2] which can reach a base temperature of 330mK. The samples in this fridge sit in a sample space, which is surrounded by a ^{3}He bath. This, in turn, is thermally coupled to the sample space via ^{3}He exchange gas. Cooling samples to base temperature is done by a charcoal sorption pump cooled by a ^{4}He 1K pot.
Josephson tunnel junction and SQUID tips were measured in a commercial Oxford Heliox fridge[3], with a base temperature of < 300mK. In this fridge samples are immersed in liquid ^{3}He.

3.3.1 Filtering

At low temperatures, electron cooling by the substrate, i.e. by phonons, is rather bad. Even if the cooling power of ^{3}He systems is in the range of hundreds of μW, it could be that the substrate itself will be cold, while the electrons will still be hot. This requires us to consider the effect of all sources of electron heating, the main agent of which is electromagnetic radiation propagating through the wires from room-temperature environment to the sample space lying

2 Designed by Michael Reznikov, now at the Technion, and built in Chernogolovka near Moscow.
3 `http://www.oxinst.co.uk`

at the base temperature [32, 33]. To minimize em radiation from room-temperature, we built a new rod for the home-made ^{3}He system which employs some of the key principles in low-temperature filtering [34, 32]. A few pictures of this rod are given in fig. 3.7. To reduce

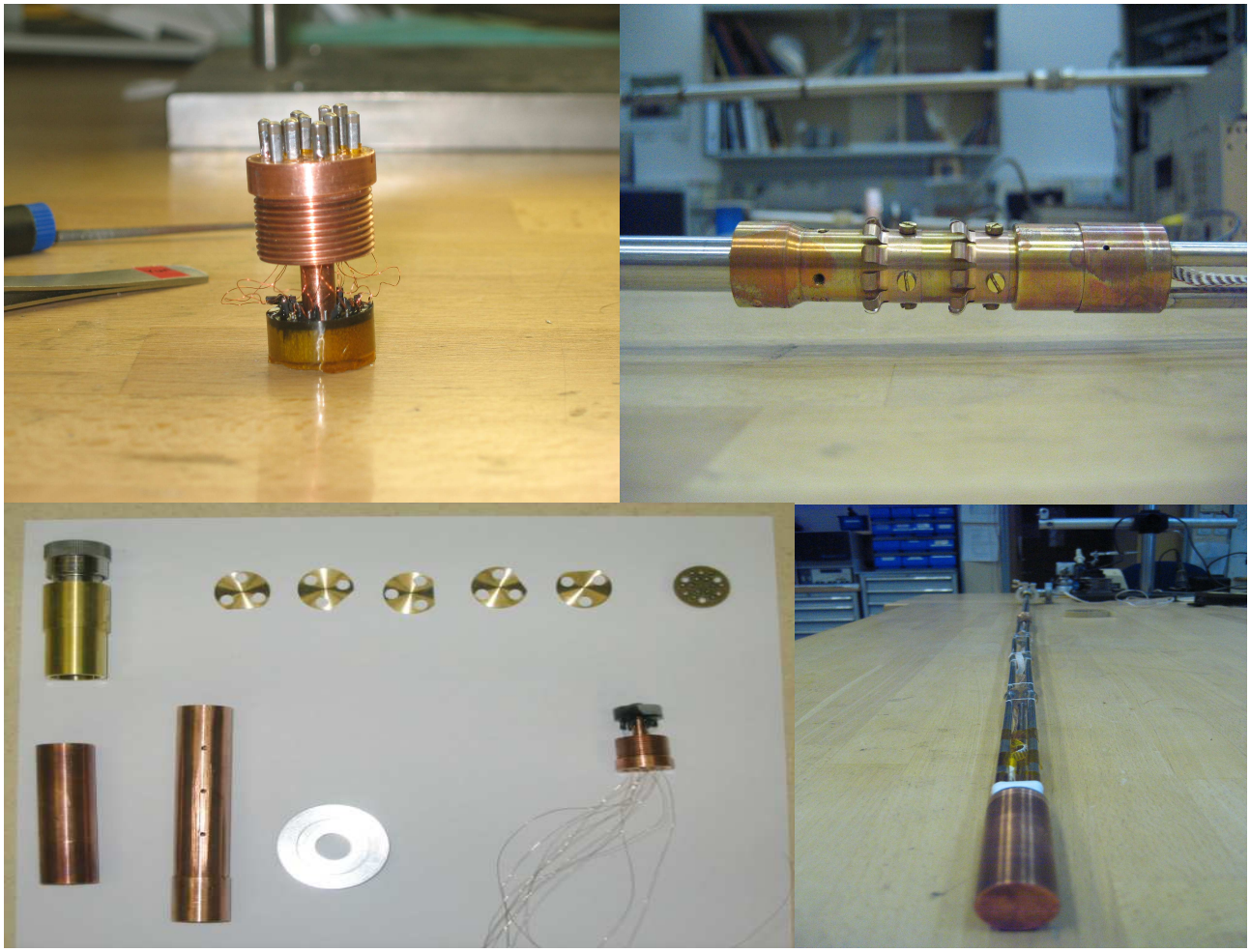

Fig. 3.7: *Top-left: The bottom part of the Faraday cage. All the π-filters are sticking out of it (before soldering to the manganin ribbon of wires). Top-right: A close-up of the copper thermal coupler to the 1K pot. Bottom-left: some of the parts which comprise the rod. The big copper piece couples the sample space to the 1K pot via a set of BeCu springs. Bottom-right: complete rod.*

heat load due to thermal conductivity, thin-walled stainless steel rods (od 5mm, id 4.5mm) comprise half of the rod, and are connected to a massive copper piece thermally coupled to the liquid-^{4}He pot. This ensures that the gradient will be only from 4.2K to 300mK instead of room-temperature to 300mK. In addition, instead of using standard copper wires, we used twisted pairs of Manganin wires[4] which have bad thermal conductivity, so that they, too, limit

4 `http://www.cryoconnect.com`

the heat load from the environment to the base temperature region. Due to their bad thermal conductivity, these wires also have bad electrical conductivity (Wiedemann-Franz law), which means that for this rod, each wire has a resistance of 180Ω. Rf-filtering at low-temperatures is done using π-filters[5], which have no resistive components. All manganin wires from the room-temperature connector are soldered to one side of the filters, its base soldered to the bottom of a copper Faraday cage. The wires from the other side of the filters connect to a 24-pin socket, onto which the tip-holder is plugged.

3.4 Helium-4, 1.5K-300K system

We use 1.5K-300K cryostats which are placed inside a 6T Cryomagnetics magnet in a 100 liter ^{4}He Cryofab Dewar. There is a needle valve which enables us to control the helium flow from the Dewar to the cryostat. The temperatures of both the cryostat and the rod are controlled by two Lakeshore 330 temperature controllers.

3.5 SPM

All scanning measurements were done in an Omicron[6] custom-made surface probe microscope. The microscope sits inside an ultra-high vacuum chamber, which is coupled through copper plates to a ^{3}He pot with a base temperature of 350mK. Coarse movement in the z direction (towards the sample) is achieved using saw-tooth operated sliding teeth which grab the sample-holding block. Fine transverse and z movements are achieved using piezoelectric elements.
We use the SPM in STM-mode. In STM, to approach a sample a 1V voltage is applied on it and the tunneling current through the tip is measured back to a feedback loop which controls the z movement of the sample. A schematic diagram of the circuit is displayed in fig. 3.8.

3.6 Electronics, data gathering & analysis

3.6.1 Continuous tips

An ac current is applied to the tip from the oscillator of a 7260 EG&G lock-in amplifier through a resistor and the voltage difference between the two leads of it is measured back in the lock-in amplifier. To measure the effect of dc current bias, a Yokogawa 7651 is connected in series with

5 Tusonix 4701-001, `http://www.tusonix.com/smt`

6 `http://www.omicron.de/index2.html`

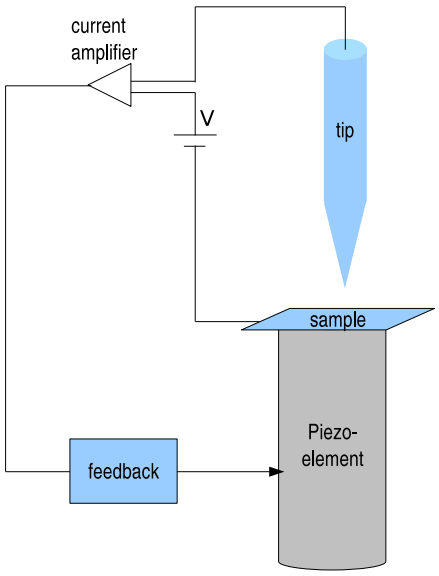

Fig. 3.8: *Schematic diagram of the feedback loop in the SPM.*

the oscillator and effectively the differential resistance is measured in the lock-in amplifier. The 6T magnet was fed by a Toellner 8805 power supply.

3.6.2 Quantum interference device tips

All Josephson junction and SQUID measurements were done in voltage bias. That is to say, a voltage bias was applied on the tip using a standard Yokogawa 7651 dc source and the current through it was amplified using an Ithaco 1211 current amplifier[7] to a voltage which was read by an Agilent 34401A multimeter. Ac measurements were done in a similar way to the continuous tip, i.e. an ac-source (usually the oscillator of an SRS830 lock-in amplifier) was connected in series with the dc source, and the current was measured by the current measurement circuit of the lock-in amplifier[8]. Effectively, then, we measured the differential conductance of the tip. According to sec. 2.1, this is a direct measurement of the density of states, from which we can deduce the superconducting gap Δ and the normal state resistance R_n.

7 typical amplification is $10^{-6} - 10^{-8}$ A/V.

8 SRS830 lock-in amplifiers have a fixed amplification of either 10^{-6} or 10^{-9} A/V.

4. Results

4.1 Aluminium Tips

4.1.1 Continuous film tips

Before making any "weak link"-based device, we first wanted to characterize a $\sim$ 20nm thick continuous film on a tip. The superconducting phase transition gives us an estimate of T_c, from which we calculate the energy gap, $\Delta(0) = \frac{\pi}{e^\gamma} k_B T_c$, with γ being the Euler number. We present measurements of the effective differential resistance of a tip with a diameter of 100nm in fig. 4.1. Note the "jump" in the dc measurement presented in fig. 4.1a. This is the mark of superconductivity being quenched. At currents smaller than this critical current I_c, the tip is superconducting and its resistance is zero, while at currents larger than I_c, superconductivity is quenched and its resistance jumps to its normal state resistance R_n. Ac measurements of the same tip exhibit a peak in the differential resistance in the region of the critical current.

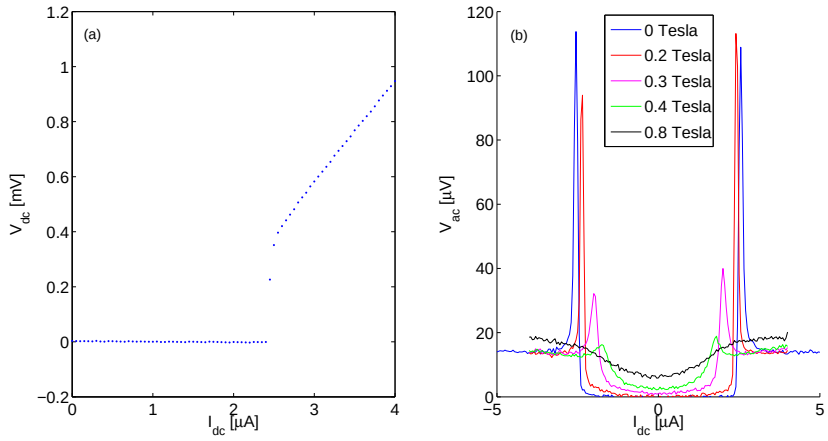

Fig. 4.1: *(a) Dc I-V measurement of a continuous thin aluminium film tip. 360Ω wire resistance was subtracted; (b) Differential resistance measurements of a continuous thin aluminium film tip for different magnetic fields. The ac current amplitude was 50nA@10.5Hz. Note the decrease in the critical current with magnetic field. In all curves a constant 360Ω of wire resistance was subtracted.*

We expect that magnetic field will make the critical current decrease until superconductivity is completely quenched in the tip, observed in fig. 4.1b.

The sharp feature of such a tip is also its downside: It is very sensitive to magnetic field *only* in the region near the critical field. One could tune this region a bit by working in different dc current biases, but even then it gives no magnetic field dependence at low fields.

The largest slope of an ac measurement at the critical field we got was $\sim 1\mu V/\text{Gauss}$ (at a frequency of 10.5 Hz). Dc measurements gave similar slopes. Depending on our electronics, of course, we see that the best sensitivity achieved in this case is a few $\text{Gauss}/\sqrt{\text{Hz}}$. A more detailed discussion on senstivity estimates will be given in chapter 5.

4.1.2 Josephson junction tips

The first successful tips measured had a diameter of 100nm. These tips were evaporated usually with the 2nd junction geometry (see sec. 3.1.2). We changed only the O_2 pressure during oxidation to optimize their performance, i.e. increase their maximum supercurrent. They showed interesting subgap features, illustrated in fig. 4.2. It is important to note that the lowest

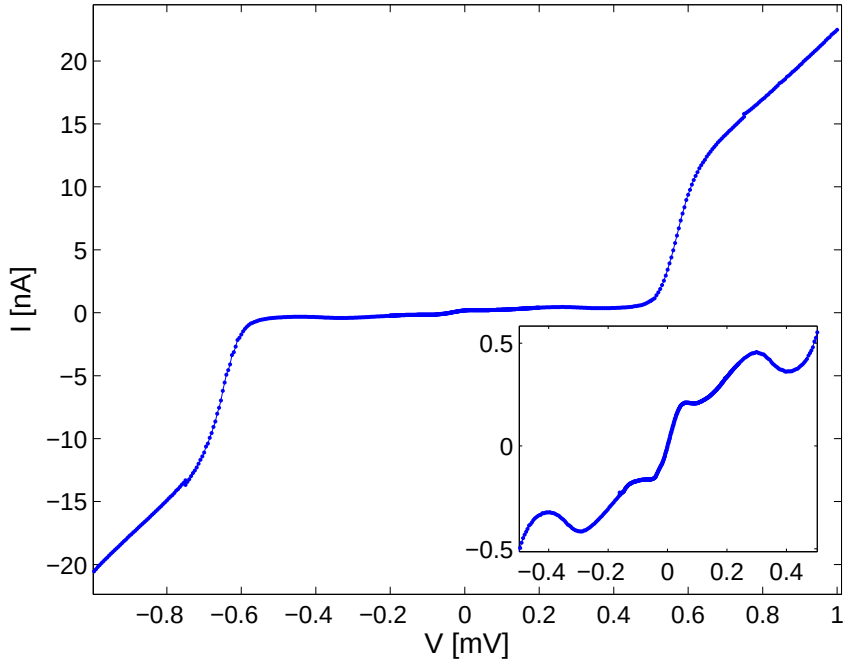

Fig. 4.2: *An $Al/Al_2O_3/Al$ single tunnel junction tip. Inset: the subgap features.*

normal state resistance we got with this tip size was $R_n = 50\text{k}\Omega$ at base temperature. For this R_n, the Josephson energy is $E_J \sim 16\mu\text{eV}$, which is smaller than k_BT at $T = 300\text{mK} = 26\mu\text{eV}$.

In the phase fluctuation regime [35], the Josephson supercurrent appears at a finite voltage bias, and the I-V curve in the near vicinity of the zero bias can be fitted by eq. 2.16. Following Na'aman et al. [35], we define two parameters, $A \equiv \frac{1}{2} I_{c0} Z_1$ and $V_p \equiv 2eZ_1 k_B T/\hbar$. We took four I-V curves of similar tunnel junction tips near the zero voltage bias and fitted them using eq. 2.16 and the two parameters, A, V_p. An example of such a fit is given in fig. 4.3.

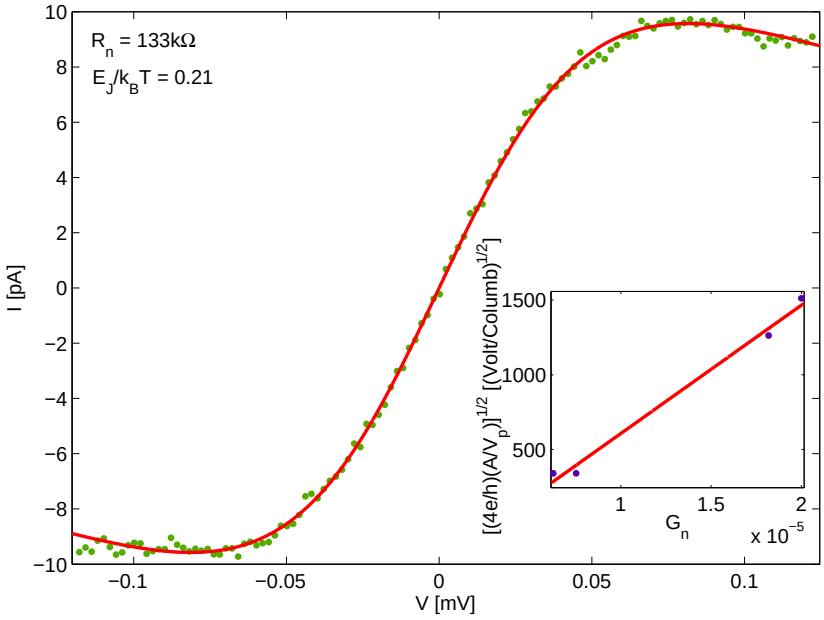

Fig. 4.3: *Phase diffusion regime fit to measurements for a small single tunnel junction tip; Inset: the ratio between A and V_p of four tips is plotted here as a function of the normal state conductance. A fair linear fit connects the points, which leads to one environment temperature for the system.*

To see whether this fit is reasonable, we plotted $\sqrt{(4e/\hbar)A/V_p}$ as a function of $G_n = 1/R_n$ in fig. 4.3 for four tips.

Calculating the slope, we see that it is

$$\sqrt{(4e/\hbar)A/V_p}/G_n = \frac{I_{c0}R_n}{\sqrt{k_B T}} = \frac{\pi\Delta/2e}{\sqrt{k_B T}}.$$

The units used are Ampère for I_{c0}, Volts for V_p and Ohm^{-1} for G_n, so that the units for the slope are $\left[\sqrt{\frac{\mathrm{Volt}}{\mathrm{Columb}}}\right]$. The effective temperature the junctions "see" is therefore $T = 1.5\mathrm{K}$ and an environment impedance of $Z_1 \sim 5k\Omega$. This agrees with our experimental setup and further confirms the validity of the fit. In addition, in all four tips the peak in the supercurrent appears at the same voltage bias.

We wanted to see whether there is an interference pattern in the magnetic field dependence of these supercurrent peaks. An example of such a measurement is displayed in fig. 4.4. It

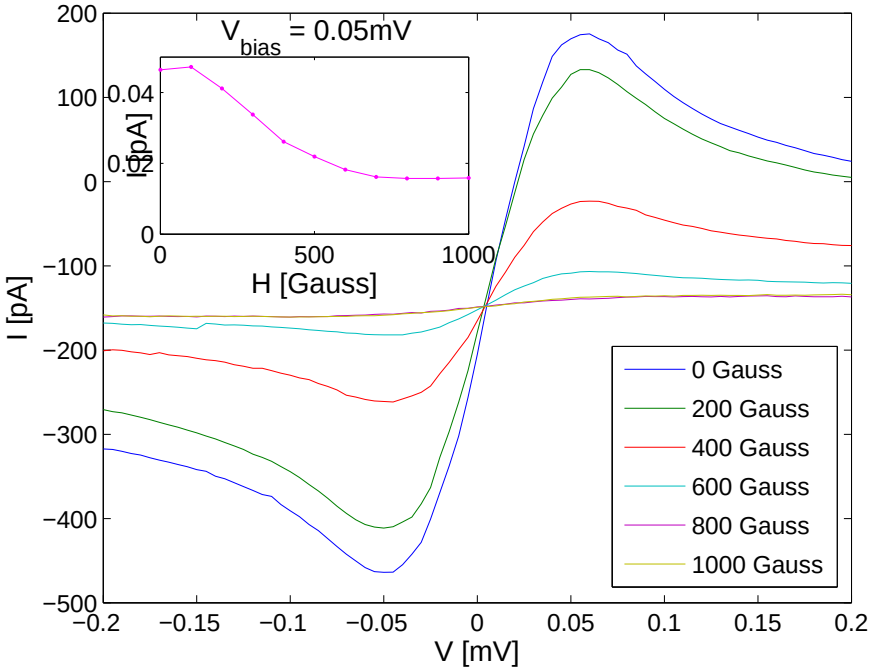

Fig. 4.4: *Magnetic field dependence of a typical 100nm x 100nm single tunnel junction tip. A decay in the supercurrent is observed. At 1000 Gauss the tip was still fully superconducting, i.e. its gap was still 250μeV. Inset: magnetic field dependence at the supercurrent peak.*

seems that the supercurrent simply decays with magnetic field. However, the complete subgap feature of the tip did not change by much, i.e. superconductivity was still intact. This could be explained if we consider the expected period in the interference pattern, calculated from the tip's diameter, $\phi = 100\text{nm} \Rightarrow \text{Period} = \Phi_0/\pi\phi^2/4 \sim 2540$ Gauss. This result means that this observed decay is simply the decrease in the maximal supercurrent when one "sits" in the zeroth-order peak of fig. 2.6. We tried making larger tips with a diameter of 500nm. The reasoning is that these larger tips will have a smaller normal state resistance and thus a larger supercurrent. However, larger tips would also mean worse spatial resolution. When measuring these larger tips we observed several interesting phenomena in the magnetic field dependence:

1. A non-monotonous dependence. There are even distinguishable minima and maxima in some of the samples.

2. Abrupt jumps in certain, reproducible values of magnetic field.

3. Hysteresis.

4. A decrease in the amplitude of the supercurrent peak as a function of the oxide layer.

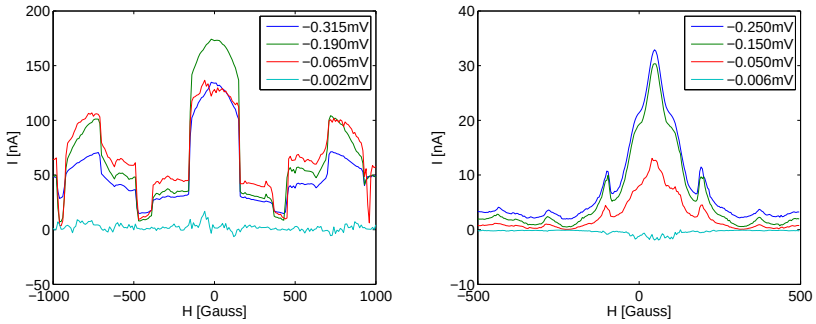

Fig. 4.5: *Magnetic field dependence of a 500nm x 500nm $Al/Al_2O_3/Al$ tunnel junctions: Left figure - magnetic field dependence for different dc biases. Note the jumps. Right figure - same measurements for a different tip.*

Fig. 4.5b shows distinct periodic minima and maxima. We tried fitting it with a rectangular Josephson junction magnetic field response curve, similar to fig. 2.6. The fit is given in fig. 4.6. Assuming what we see in fig. 4.5b is indeed an interference pattern, we can calculate the

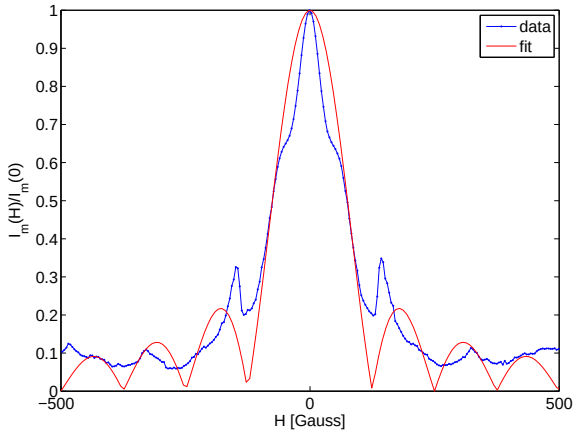

Fig. 4.6: *A rectangular Josephson junction fit to a measured tip.*

junction's area from the period. The period is 100 Gauss, which makes the junction's area $A = \Phi_0/100 = 2 \cdot 10^{-9}\text{cm}^2$. From the junction's area we can estimate the tip diameter, $\phi = 2\sqrt{A/\pi} = 285\text{nm}$, which is close to the actual diameter of the tip.
However, there are some problems with this assumption. First, a contradiction with this assumption/calculation: The junction we evaporated was placed perpendicular to the magnetic field and not parallel. A magnetic field perpendicular to a Jopsephson junction should not induce such interference effects. Second, we did not see the periodic pattern in all of the large tips. Nevertheless, it might be explained if we assume that the junction is made of small grains of aluminium. In this case, each grain has a slightly different critical current and critical field,

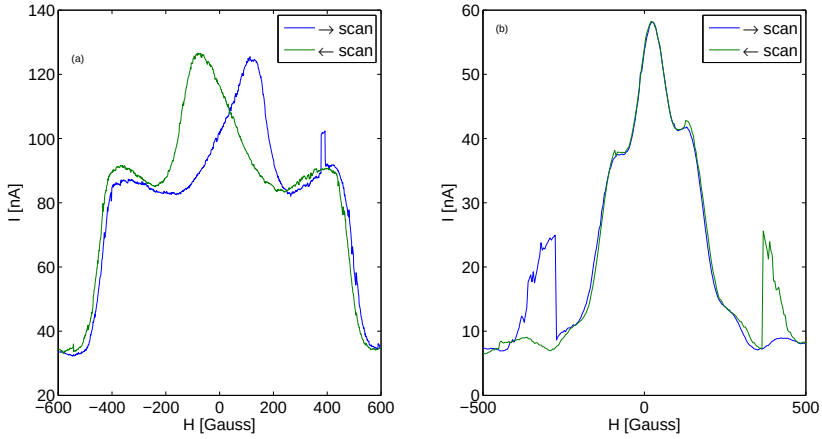

Fig. 4.7: *Hysteresis in magnetic field dependence of the subgap current. (a) A tip which was measured in the SPM before approach; (b) A tip measured in the ^{3}He system. Note the abrupt jumps.*

i.e. different characteristics, so that having several grains connected together is not necessarily the same as a homogeneous superconducting film. In addition, we tried increasing the amplitude of the supercurrent peak by making the oxide layer between the two supercondcutors thinner. As a result, not only did we not observe an increase in the supercurrent, but we actually observed a decrease. We think that this is due to the fact that we had little control over the exact oxidation rate, thus getting a different and unknown oxidation rate at each tip-making.

The differences between the tips displayed in fig. 4.5 is the background pressure during oxidation, which was 140 and 80 mTorr, respectively. Moreover, the "jumps" due to the magnetic field show a hysteretic behavior, i.e. if we scan the magnetic field from different directions, the jump will occur at different places, too. This is illustrated in fig. 4.7.

One possible explanation for these jumps is that at each jump another fluxoid enters/leaves the junction or that the fluxoid configuration in the junction changes. These effects should be observed when the size of the superconductor is of the order of or larger than its coherence length [36, 37].

To conclude, small tunnel junction tips exhibited only the first order of the interference pattern while the larger ones showed interference pattern for magnetic field dependence. The magnetic field dependence had a typical dc slope of ∼500 pA/Gauss for the supercurrent in the large diameter tips and several orders of magnitude less for the smaller diameter tips. With a proper current amplifier we can resolve (depending on the amplification) at least tens of pA, which should, in principle, give us a sensitivity of $\sim 0.1\text{Gauss}/\sqrt{\text{Hz}}$.

4.1.3 SQUID tips

As was previously mentioned in sec. 3 in detail, we attempted to make a SQUID on a tip using quartz tubes pulled to a small diameter. Our assumption was that the geometry of such a hollow tip would naturally give us the needed conditions to fabricate a SQUID, i.e. evaporating the tip from above will create two Dayem bridges (weak-links) between the two superconducting leads.

Moreover, high-quality SQUIDs are hysteretic in nature [25], and in order to use them in a practical system, they are usually shunted. In our case we presume to think that the evaporation process creates an intrinsic shunt in parallel with the SQUID. We present measurements of a SQUID on a tip with a diameter of 300nm. We measured its critical current's magnetic field dependence in two methods. For SQUIDs with an intrinsic shunt, we were in the non-hysteretic regime, thus being able to measure the critical current at a constant voltage bias. For SQUIDs without this shunt, we needed to measure the entire IV curve for each magnetic field, identify the critical current I_c and then plot it as a function of magnetic field[1]. These measurements and calculations are given in the following figure in a clear and concise form:

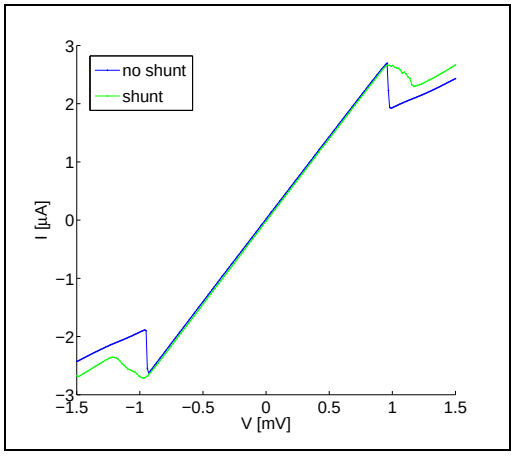

Fig. 4.8: *IV curves of a shunted an unshunted SQUID on a tip.*

The period of oscillations in fig. 4.9, 300 Gauss, agrees with the outer diameter of the tube, 300 nm (A period of 300 Gauss should give a SQUID diameter of 290 nm). The above SQUID on a tip is reproducible and it always has an intrinsic shunt. As this shunt was highly sensitive and eventually disappeared (see fig. 4.8), we performed most of our measurements on unshunted or externally shunted SQUIDs.

Upon fabricating a successful SQUID on a tip, we tried to find its magnetic field sensitivity in the ^{3}He system. This, of course, depended on the stability of the magnet's power supply. We were able to resolve 1 and 5 Gauss steps of the magnet's power supply.[2] The signal had a 1 Gauss stability over time.

Another measurement setup involved a quasi-4-wire current bias measurement. In that

1 See ref. [9] for more details.

2 Oxford IPS-120-10, with a minimal resolution of 1mA for a 1 mA/Gauss conversion ratio.

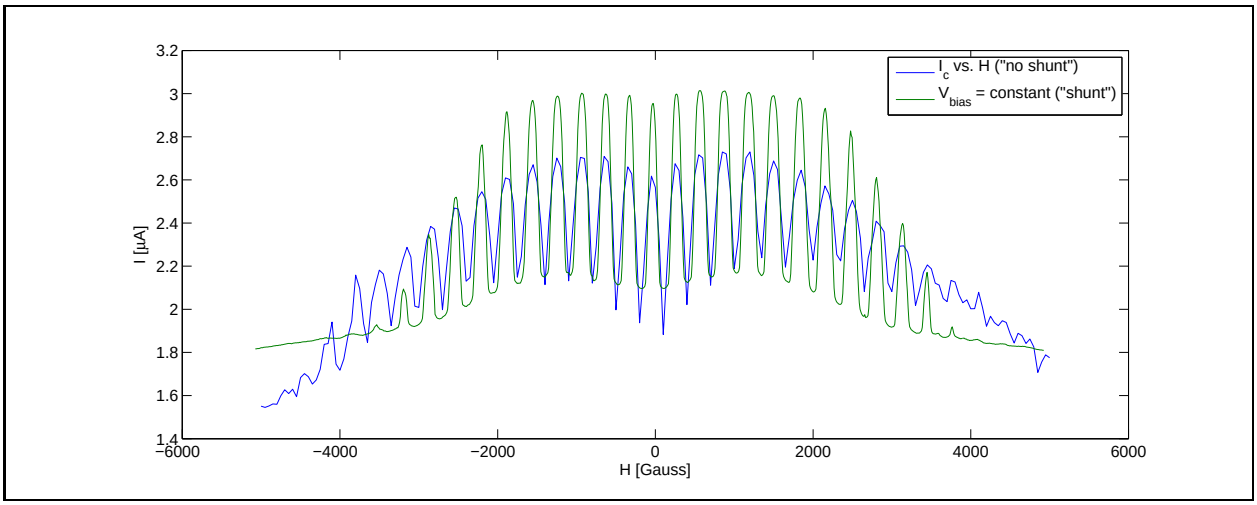

Fig. 4.9: *Magnetic field dependence of a SQUID on a tip with a diameter of 300nm.*

setup, we were able to observe the characteristic zero voltage state and the onset of voltage at the critical current. These measurements were done with an external shunt connected in parallel with the tip to inhibit hysteresis. An example of such a measurement is given in the following figure, using a 24Ω shunt for a 400Ω normal state resistance SQUID on a tip: Performing differential resistance (ac+dc) measurements enabled us to measure the magnet power supply's 1 Gauss steps with great ease at frequencies as high as 5kHz and greater (see fig 4.10). Noise measurements at different frequencies up to 20kHz yielded a noise figure of $\sim$50mG/$\sqrt{\text{Hz}}$. This number was calculated by measurements of the noise level at different frequencies with a time-constant of 300ms. The noise level was 160mG, so that by multiplying it by the time constant we got 48mG/$\sqrt{\text{Hz}}$.

4.2 Niobium Tips

4.2.1 Continuous film tips

We managed to make a superconducting continuous niobium film on a $\phi = 100$nm tip. Its critical current was relatively high, $I_c = 130\mu$A, and its critical field $H_c = 4000$ Gauss (see fig. 4.11).

This is just the first step in making niobium tips. We planned to proceed to Josephson junctions and SQUIDs but in this project's time frame were not able to do so.

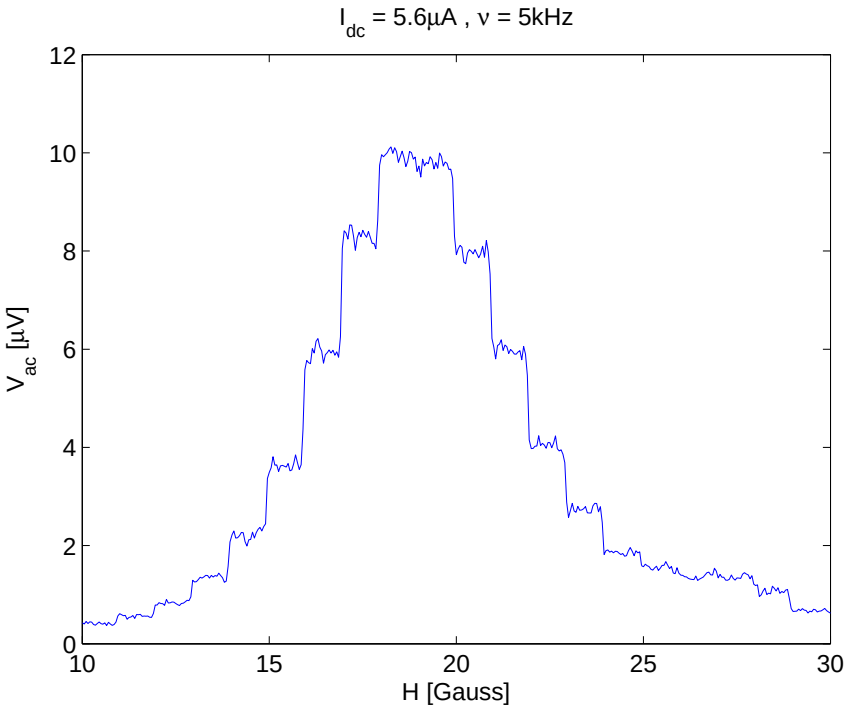

Fig. 4.10: *Clear 1 Gauss steps observed in a differential resistance measurement at a frequency of 5kHz.*

4.3 SPM

With SET tips, it is possible to approach the surface of a sample using Coulomb Blockade oscillations (CBO)[10]. In our case, however, we needed to devise a different approach technique. As a first, naïve, attempt, we tried to approach the sample using the original STM technique built into the microscope. As a test sample we chose a few micron thick crystal of $NbSe_2$, which we wanted to scan with our tip at a constant external magnetic field to observe vortices. The assumption was, that we would be able to identify a tunneling current between the end of the tip and the sample. However, at first we did not manage to actually approach the surface of a sample with a tip. These attempts ended in a crash at the end of the approach sequence. We understood that the current approach technique, using tunneling between the tip's end and the sample, was simply not adequate, presumably because of a thin layer of alumina which is created on the top-most layer of the aluminium film due to oxidation. Three possible solutions were proposed:

1. Assuming that tunneling is not very reliable due to oxidation of the aluminium near the end of the tip, coat the aluminium with Au or Pd-Au on-top. Gold and also palladium do not oxidize, so that this additional layer should make tunneling more reliable. This

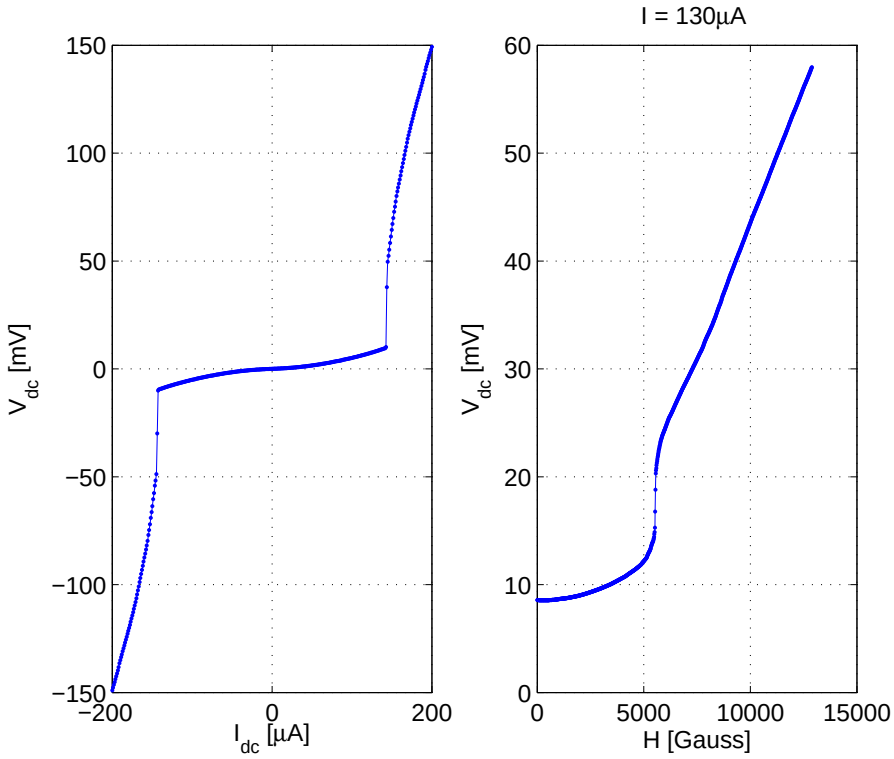

Fig. 4.11: *Left: I-V measurement of a continuous film niobium tip. Right: Magnetic field dependence at a current bias near slightly below the critical current.*

solution proved to be successful, and we did manage to approach samples with Josephson junction tips.

2. Use an alternative method for approach. For example, tuning-fork force-microscopy [9] has been suggested.

3. Use the in-situ preparation chamber of the SPM to fabricate samples so that the aluminium cannot oxidize during and after the evaporation.

As continuous film tips were just an intermediate stage and regardless had unsatisfactory SNR, we did not pursue any of these alternatives for this kind of tips. However, we did attempt to apply the first proposal to the Josephson junction tips.

5. Discussion

Our goal was to fabricate a sensitive magnetic field probe on a tip with which we wanted to image vortices. In such a way we aim to explore vortex matter and possibly vortex dynamics. In the following sections we will discuss our results and see whether we have achieved our goal.

5.1 Sensitivity Comparison

In general, we managed to observe the minimal resolution of the power supply (1 Gauss) only with the SQUIDs. As intermediate steps, both the continuous and the Josephson tips contributed much to our understanding, but failed to give a reliable and sensitive enough signal. We summarize the different tips' characteristics in the following table:

Tip Device	Sensitivity[1]	Pros	Cons
Continuous	1 Gauss/$\sqrt{\text{Hz}}$	Good SNR	Sensitive only at the critical field region
Josephson (s)	1 Gauss/$\sqrt{\text{Hz}}$	None	Sensitive only at the coherence peaks
Josephson (l)	$<$ 1 Gauss/$\sqrt{\text{Hz}}$	Modulation	Jumpy signal; Irreproducible; Hysteretic
SQUID	50 mG/$\sqrt{\text{Hz}}$	Modulation; Low fields	Hysteretic[2]

[1] The sensitivity given in the above table refers to the effective sensitivity attained in our measurement setup with this tip.

[2] Can be easily solved by shunting the SQUID. [3] (s) and (l) in lines (2) and (3) refer to small and large diameter tips, respectively.

5.2 Future Prospects

We intend to continue exploring SQUIDs on a tip, as these tips show great promise in the field of scanning probe microscopy combined with magnetic flux measurements. To further explore

vortex matter with these tips, we plan to construct a scanning SQUID microscope using either aluminium or niobium SQUIDs as the chief sensors.

5.3 Comparison with "Commercial" SQUIDs

For a 300nm ring, each period (Φ_0) is ~300 Gauss. A 0.05 Gauss/$\sqrt{\text{Hz}}$ sensitivity is equivalent, then, to a resolution of $\sim 10^{-4}\Phi_0/\sqrt{\text{Hz}}$. The best SQUIDs up-to-date [7] have a sensitivity of $\sim 10^{-6}\Phi_0$, but these devices use a flux-locked loop (FLL) and a coupling flux transformer near the sample, keeping the SQUID itself in a quiet, well-shielded environment. We think it might be possible to achieve a much better magnetic field sensitivity with our SQUID using better electronics and quieter magnetic field power supplies.

References

[1] Bednorz, J. G. and Müller, K. A. Possible high-T_c superconductivity in the BaLaCuO system. *Zeitschrift für Physik B Condensed Matter* **64**, 189–193 (1986).

[2] Abrikosov, A. A. On the magnetic properties of superconductors of the second group. *Soviet Physics Journal of Experimental and Theoretical Physics* **5**, 1174–1182 (1957).

[3] Brandt, E. H. Precision Ginzburg-Landau solution of ideal vortex lattices for any induction and symmetry. *Phys. Rev. Lett.* **78**(11), 2208–2211, Mar (1997).

[4] Brandt, E. H. Ginzburg-Landau vortex lattice in superconductor films of finite thickness. *Physical Review B (Condensed Matter and Materials Physics)* **71**(1), 014521 (2005).

[5] Essmann, U. and Träuble, H. The direct observation of individual flux lines in type II superconductors. *Physics Letters A* **24**, 526–527 (1967).

[6] Goa, P. E., Hauglin, H., Baziljevich, M., Il'yashenko, E., Gammel, P. L., and Johansen, T. H. Real-time magneto-optical imaging of vortices in superconducting $NbSe_2$. *Superconductor Science and Technology* **14**(9), 729–731 (2001).

[7] Kirtley, J. R., Ketchen, M. B., Stawiasz, K. G., Sun, J. Z., Gallagher, W. J., Blanton, S. H., and Wind, S. J. High-resolution scanning SQUID microscope. *Applied Physics Letters* **66**(9), 1138–1140 (1995).

[8] Bending, S. J. Local magnetic probes of superconductors. *Advances in Physics* **48**, 449–535 (1999).

[9] Hasselbach, K., Veauvy, C., and Mailly, D. MicroSQUID magnetometry and magnetic imaging. *Physica C: Superconductivity* **332**(1-4), 140–147 (2000).

[10] Yoo, M. J., Fulton, T. A., Hess, H. F., Willett, R. L., Dunkleberger, L. N., Chichester, R. J., Pfeiffer, L. N., and West, K. W. Scanning Single-Electron Transistor Microscopy: Imaging Individual Charges. *Science* **276**(5312), 579–582 (1997).

[11] Tinkham, M. *Introduction to Superconductivity.* Dover, New York, second edition, (1996).

[12] Josephson, B. D. Possible new effects in superconductive tunnelling. *Physics Letters* **1**, 251–253 (1962).

[13] Likharev, K. K. Superconducting weak links. *Rev. Mod. Phys.* **51**(1), 101–159, Jan (1979).

[14] Steinbach, A., Joyez, P., Cottet, A., Esteve, D., Devoret, M. H., Huber, M. E., and Martinis, J. M. Direct measurement of the Josephson supercurrent in an ultrasmall Josephson junction. *Phys. Rev. Lett.* **87**(13), 137003, Sep (2001).

[15] Ambegaokar, V. and Halperin, B. I. Voltage due to thermal noise in the dc Josephson effect. *Phys. Rev. Lett.* **22**(25), 1364–1366, Jun (1969).

[16] Falco, C. M., Parker, W. H., Trullinger, S. E., and Hansma, P. K. Effect of thermal noise on current-voltage characteristics of Josephson junctions. *Phys. Rev. B* **10**(5), 1865–1873, Sep (1974).

[17] Joyez, P., Vion, D., Gz, M., Devoret, M. H., and Esteve, D. The Josephson effect in nanoscale tunnel junctions. *Journal of Superconductivity* **12**(6), 757–766 (1999).

[18] Martinis, J. M. and Nahum, M. Effect of environmental noise on the accuracy of Coulomb-blockade devices. *Phys. Rev. B* **48**(24), 18316–18319, Dec (1993).

[19] Ingold, G.-L., Grabert, H., and Eberhardt, U. Cooper-pair current through ultrasmall Josephson junctions. *Phys. Rev. B* **50**(1), 395–402, Jul (1994).

[20] Harada, Y., Takayanagi, H., and Odintsov, A. A. Cooper-pair tunneling in small junctions with tunable Josephson coupling. *Phys. Rev. B* **54**(9), 6608–6613, Sep (1996).

[21] Ivanchenko, Y. M. and Zil'berman, L. A. The Josephson effect in small tunnel contacts. *Soviet Physics JETP* **28**(6), 1272–1276 (1968).

[22] Buckner, S. A., Chen, J. T., and Langenberg, D. N. Current-Voltage characteristics of small Josephson tunnel junctions. *Phys. Rev. Lett.* **25**(11), 738–741, Sep (1970).

[23] Jaklevic, R. C., Lambe, J., Silver, A. H., and Mercereau, J. E. Quantum interference effects in Josephson tunneling. *Phys. Rev. Lett.* **12**(7), 159–160, Feb (1964).

[24] Jaklevic, R. C., Lambe, J., Mercereau, J. E., and Silver, A. H. Macroscopic quantum interference in superconductors. *Phys. Rev.* **140**(5A), A1628–A1637, Nov (1965).

[25] Clarke, J. and Braginski, A. I. *The SQUID Handbook: Fundamentals and Technology of SQUIDs and SQUID Systems, Volume I.* Wiley-VCH, Berlin, first edition, (2004).

[26] Valaskovic, G. A., Holton, M., and Morrison, G. H. Parameter control, characterization, and optimization in the fabrication of optical fiber near-field probes. *Applied Optics* **34**, 1215 (1995).

[27] Essaidi, N., Chen, Y., Kottler, V., Cambril, E., Mayeux, C., Ronarch, N., and Vieu, C. Fabrication and characterization of optical-fiber nanoprobes for scanning near-field optical microscopy. *Applied Optics* **37**, 609–615 (1998).

[28] Yoshii, K., Yamamoto, H., Saiki, K., and Koma, A. Superconductivity and electrical properties in single-crystalline ultrathin Nb films grown by molecular-beam epitaxy. *Phys. Rev. B* **52**(18), 13570–13575, Nov (1995).

[29] Wildes, A. R., Mayer, J., and Theis-Bröhl, K. The growth and structure of epitaxial niobium on sapphire. *Thin Solid Films* **401**(1-2), 7 (2001).

[30] Wolf, S. A., Qadri, S. B., Claassen, J. H., Francavilla, T. L., and Dalrymple, B. J. Epitaxial growth of superconducting niobium thin films by ultrahigh vacuum evaporation. *Journal of Vacuum Science & Technology A: Vacuum, Surfaces, and Films* **4**(3), 524–527 (1986).

[31] Quateman, J. H. T_c suppression and critical fields in thin superconducting Nb films. *Phys. Rev. B* **34**(3), 1948–1951, Aug (1986).

[32] Vion, D., Orfila, P. F., Joyez, P., Esteve, D., and Devoret, M. H. Miniature electrical filters for single electron devices. *Journal of Applied Physics* **77**(6), 2519–2524 (1995).

[33] Bladh, K., Gunnarsson, D., Hurfeld, E., Devi, S., Kristoffersson, C., Smlander, B., Pehrson, S., Claeson, T., Delsing, P., and Taslakov, M. Comparison of cryogenic filters for use in single electronics experiments. *Review of Scientific Instruments* **74**(3), 1323–1327 (2003).

[34] Martinis, J. M., Devoret, M. H., and Clarke, J. Experimental tests for the quantum behavior of a macroscopic degree of freedom: The phase difference across a Josephson junction. *Phys. Rev. B* **35**(10), 4682–4698, Apr (1987).

[35] Naaman, O., Teizer, W., and Dynes, R. C. Fluctuation dominated Josephson tunneling with a scanning tunneling microscope. *Phys. Rev. Lett.* **87**(9), 097004, Aug (2001).

[36] Geim, A. K., Grigorieva, I. V., Dubonos, S. V., Lok, J. G. S., Maan, J. C., Filippov, A. E., and Peeters, F. M. Phase transitions in individual sub-micrometre superconductors. *Nature* **390**, 259–262 (1997).

[37] Kanda, A., Baelus, B. J., Peeters, F. M., Kadowaki, K., and Ootuka, Y. Experimental evidence for giant vortex states in a mesoscopic superconducting disk. *Physical Review Letters* **93**(25), 257002 (2004).